Raman scattering in metals with disorder: beyond the zero-momentum approximation

2003 J. Phys.: Condens. Matter 15 3751

(http://iopscience.iop.org/0953-8984/15/22/309)

INSTITUTE OF PHYSICS PUBLISHING JOURNAL OF PHYSICS: CONDENSED MATTER

J. Phys.: Condens. Matter **15** (2003) 3751–3758 PII: S0953-8984(03)59064-6

Raman scattering in metals with disorder: beyond the zero-momentum approximation

E Ya Sherman[1,3] **and O V Misochko**[2]

[1] Institute for Theoretical Physics, Karl-Franzens-University, Graz, A-8010, Graz, Austria
[2] Institute of Solid State Physics, RAS, 142432 Chernogolovka, Moscow Region, Russia

Received 3 February 2003
Published 23 May 2003
Online at stacks.iop.org/JPhysCM/15/3751

Abstract

We consider inelastic light scattering (a Raman process) in non-fully symmetrical channels in metals with disorder and doped semiconductors. Due to the screened Coulomb interaction between electrons moving in the random field of impurities, the electronic excitations with relatively large momenta contribute to the Raman spectra. The physics of this effect is related to the physics of the inelastic collisions of electrons that arises due to the same interaction. We show that the contribution of the finite-momentum excitations can be regarded as a manifestation of the weak localization of carriers due to the disorder.

1. Introduction

In an inelastic light scattering (Raman) experiment, a laser beam at frequency ω illuminates the surface of a solid, and the spectrum of the scattered light is analysed as a function of the shift of the light frequency in the scattering process, Ω. The measured value in this case is the spectral density of the scattered light $\rho(\Omega)$, which is the number of the counted scattered photons in a given small energy interval per time unit. Typically, $\rho(\Omega)$ for metals and semiconductors consists of a continuum (a smooth function of Ω) and some peaks, corresponding to phonon excitations. In this paper we will be interested in the continua which are formed by different kinds of low-energy electronic excitation [1, 2]. It is usually assumed that the momenta of the Raman-active excitations are $Q_R \sim 2\pi \max(1/\lambda, 1/\delta)$, where δ is the light penetration depth, and λ is the photon wavelength (we put $\hbar \equiv 1$). Q_R defined in this way is more than two orders of magnitude smaller than the Fermi momentum k_F. This smallness often allows one to assume that these excitations have zero momenta and to put $Q = 0$ for the excitations in the calculations of Raman response. The effect of such small momentum transfer caused by the finite penetration depth in metals has been investigated by Falkovsky [3]. In the approach of [3], light is scattered by the electrons moving at the large spatial scale $\delta \gg \ell$ diffusively

[3] On leave of absence from: The Moscow Institute of Physics and Technology, 141700, Dolgoprudny, Moscow Region, Russia.

0953-8984/03/223751+08$30.00

rather than ballistically (ℓ is the electron free path). The energy of these excitations is given by $\sim DQ^2$, and the corresponding Raman shift is of the order of $D\delta^{-2}$, where the diffusion coefficient $D = v_F^2\tau/3$ (v_F is the Fermi velocity, τ is the electron elastic relaxation time assumed to be momentum independent, and $\ell = v_F\tau$). However, in the presence of disorder, the momentum conservation rule leading to small Q_R is broken. The role of the breakdown was for the first time recognized by Shuker and Gammon [4], who considered Raman scattering by atomic vibrations in glasses. In accordance with the approach of [4], the spatial coherence of the vibrations is characterized by a length Λ estimated to be approximately 400 Å—that is, about 0.1λ. All vibrations with momenta in the range $0 \leqslant Q < 2\pi/\Lambda$ contribute almost equally to the Raman response, and the spectral density of scattered light has no contribution distinguishable from that of the $Q_R \sim 2\pi/\lambda$ excitations. On the basis of their consideration, Shuker and Gammon calculated the spectral density of scattered light, thereby explaining a Raman band extending up to 600 cm^{-1}.

Itai [5] considered light scattering by coupled electron–phonon excitations in metals with impurities and showed that, due to conservation of total momentum in the Raman process, Raman-active excitations can consist of electron–hole pairs and phonons with opposite finite momenta. The purpose of this paper is to consider the effect of excitations with $Q \gg 2\pi \max(1/\delta, 1/\lambda)$ arising due to electron–electron interaction on electronic Raman scattering in non-fully symmetrical polarizations in three-dimensional (3D) metals and doped semiconductors with disorder. We shall refer to such excitations as 'finite-momentum' excitations and show that the influence of disorder on electronic Raman scattering is different from the effects discussed for the vibrations in [4], since there is still a distinguishable contribution from the zero-momentum excitations. This is valid even when the scale at which the momentum conservation is broken—that is, ℓ—is so small that $\ell \sim k_F^{-1}$. In the latter case the finite-Q excitations lead to corrections to the main $Q = 0$ term which can be considered within the weak-localization theory [6]. The corrections are relatively small since the weak-localization effects are small in 3D conductors.

2. Finite-momentum Raman processes

The inelastic light scattering can be considered as a process of dissipation of the energy of the external electromagnetic field in a solid due to the excitation of quasiparticles there. The frequency of the corresponding effective external perturbation, driving the system and leading to the dissipation, however, is not the frequency of the incident or scattered light, but their difference Ω. A theory of the Raman scattering in metals with impurities for $Q_R = 0$ was developed by Zawadowski and Cardona [2]. In this case the real part of the energy transfer to diffusing electrons, which is of the order of DQ^2, tends to zero, and, therefore, the Raman intensity at finite frequencies rises due to the imaginary part of the electron self-energy i/τ. The effective Hamiltonian describing the Raman process as a response to an external perturbation can be written as [2]

$$\hat{H}_R = \sum_{\boldsymbol{k},\sigma} \gamma_{\boldsymbol{k}} \hat{c}^+_{\boldsymbol{k},\sigma} \hat{c}_{\boldsymbol{k},\sigma}, \tag{1}$$

where $\gamma_{\boldsymbol{k}}$ is a Raman vertex depending on the polarization of the incident and the scattered light, the light frequency, and the crystal band-structure [7], $\hat{c}^+_{\boldsymbol{k}}$ and $\hat{c}_{\boldsymbol{k}}$ are the electron creation and annihilation operators, and σ is the spin projection. It is assumed that the photon momentum is equal to zero in $\hat{H}_R$. The light is scattered by the effective density fluctuations arising due to the $\boldsymbol{k}$-dependence of $\gamma_{\boldsymbol{k}}$, which is analogous to the mechanism of Raman scattering by the intervalley charge density fluctuations in multi-valley semiconductors [8]. Below, we

consider the case of non-fully symmetrical scattering polarizations, where the polarizations of the incident and scattered light are perpendicular to each other, and $\langle\gamma_k\rangle_{FS} = 0$, where $\langle\cdots\rangle_{FS}$ stands for the average over the Fermi surface.

The Raman spectral density, which is proportional to the dissipation rate, is related by the fluctuation-dissipation theorem to the imaginary part of Raman susceptibility $\chi_0(\Omega)$ [9]:

$$\rho(\Omega) = A[n_B(\Omega) + 1]\chi_0''(\Omega), \tag{2}$$

where $n_B(\Omega) = 1/[\exp(\Omega/T) - 1]$ is the Bose function. A is a constant that depends on many factors which can vary from one experiment to another, giving the reason for the typical presentation of $\rho(\Omega)$ in arbitrary units. The most important factor in equation (2) is $\chi_0''(\Omega)$, which can be extracted from $\rho(\Omega)$—albeit, typically, in arbitrary units, too. The Feynman graph for zero-momentum Raman polarizability is shown in figure 1. In the non-fully symmetrical scattering channels, the renormalization of the Raman vertex by isotropic impurity scattering assumed here and the vertex corrections arising due to screened Coulomb interaction vanish. The electron Green function in the diagram in figure 1 has the Matsubara form:

$$G(\varepsilon_n, \xi) = \frac{1}{\mathrm{i}\varepsilon_n - v_F\xi + \mathrm{i}/2\tau\ \mathrm{sgn}(\varepsilon_n)}, \tag{3}$$

where $\varepsilon_n = \pi T(2n + 1)$ is the fermionic Matsubara frequency, T is the temperature, and $\xi = k - k_F$. In the non-fully symmetrical Raman scattering channels, the spectral density of scattered light at $\Omega \gg T$ is given by [2]

$$\rho(\Omega) = N_F\langle\gamma_k^2\rangle_{FS}\frac{\Omega\tau}{1 + (\Omega\tau)^2}, \tag{4}$$

where N_F is the density of states at the Fermi level. Despite the broken translational symmetry due to the finite electron free path ℓ, finite-momentum excitations are not caught by this diagram. We shall consider another kind of Raman process, where the finite-momentum excitations appear in the final state. The total Raman susceptibility is the sum of two terms: $\chi(\Omega) = \chi_0(\Omega) + \chi_Q(\Omega)$, where $\chi_Q(\Omega)$ is the contribution of finite-Q excitations. The corresponding Raman process shown in figure 2 can be described as follows. A virtually excited electron creates the real electron–hole pair due to the interaction between the particles [10]. The momentum of the virtually excited electron relaxes due to the interaction with impurities in such a way that the momentum of the electron–hole pair is compensated by the momentum transferred to the crystal. Since the impurity scattering is elastic, no excitation additional to the real electron-pair energy transfer to the crystal occurs. At this point we mention three other physical effects, which have features in common with the finite-momentum Raman scattering. First, the process is analogous to the Mössbauer effect where the momentum of a γ-photon is transferred to the whole crystal but its energy remains constant because of the large crystal mass. Second, the process of finite-momentum excitations is a many-body effect analogous to the well-known shake-up process in the atomic shells. In the shake-up process the energy is redistributed between the states due to Coulomb interaction between electrons, and the final excited electronic state arises due to this interaction [11]. The comparison of the conventional Raman process and the process involving the electron–electron interaction is shown in figure 3. Third, the physics of the finite-momentum Raman process is analogous (but, of course, not identical) to the physics forming the inelastic relaxation rate of electrons τ_{ee}^{-1} due to the interaction between them. This process is shown in figure 4 where the energy of the electron near the Fermi level relaxes due to the excitation of the low-energy electron–hole pair moving in the random field of impurities $U(\boldsymbol{r})$ [6]. The Raman intensity corresponding to the process shown in figure 1 is proportional to the conversion rate of the initial photon

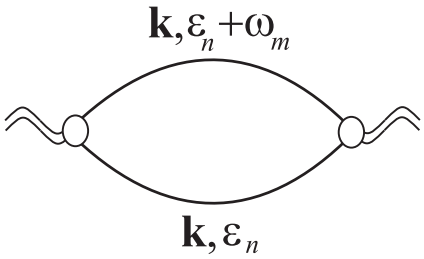

Figure 1. The Feynman graph for the zero-momentum Raman scattering. Double wavy lines correspond to the external perturbation, with white ellipses corresponding to the Raman vertex γ_k. Solid curves are the electronic Matsubara Green functions with momentum $\boldsymbol{k}$. $\omega_m = 2\pi T m$ and $\varepsilon_n = \pi T(2n + 1)$ are the bosonic and the fermionic Matsubara frequencies, respectively.

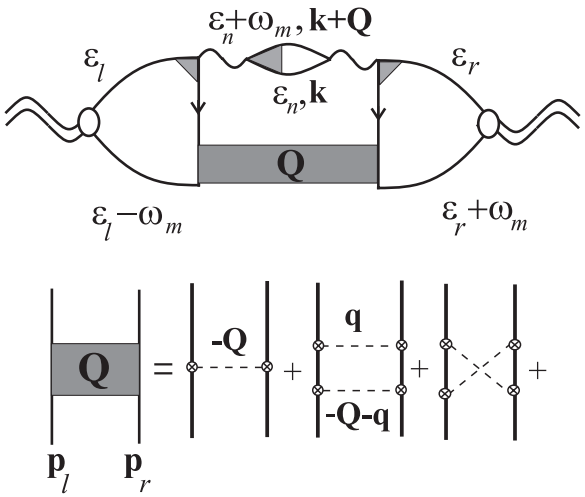

Figure 2. The Feynman graph for the finite-momentum Raman scattering. The grey rectangles correspond to the elastic momentum transfer between left (subscript l) and right (subscript r) shoulders of the diagram. The left and right Matsubara energies are defined as $\varepsilon_l = \pi T(2n_l + 1)$ and $\varepsilon_r = \pi T(2n_r + 1)$. The dashed lines connecting the white circles with the crosses inside correspond to scattering of electrons by impurities. The grey triangles show the renormalization by impurities. The simple wavy lines present the screened Coulomb interaction.

field in the zero-momentum electronic excitations and scattered photons, whereas the graph is figure 2 corresponds to the conversion in the finite-momentum excitations and scattered photons. This type of conversion arises due to the interaction between electrons. The role of electron–electron interaction in the Raman process is twofold: it changes the spectrum of carriers and leads to the finite-momentum excitations. We shall be interested in the second effect only.

3. Feynman graph calculations and results

Two main contributions related to finite-momentum excitations are the diffuson $\chi_D(\omega_m)$ and Cooperon $\chi_C(\omega_m)$, with graphs where a ladder (non-crossing impurity lines) and a fan (maximally crossed impurity lines) are inserted in the cross-section for the real excitation, as shown in figure 2—that is, $\chi_Q(\omega_m) = \chi_D(\omega_m) + \chi_C(\omega_m)$. The interaction responsible for the excitation of the final-state (real) electron–hole pair is the screened Coulomb potential taken

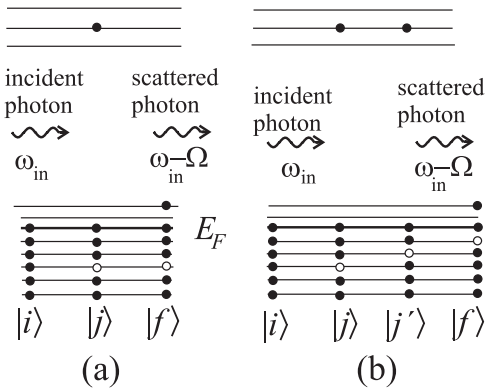

Figure 3. (a) The conventional Raman process; (b) the Raman process analogous to the shake-up process. The electronic states shown in the figure are in the random field of impurities, and, therefore, are not characterized by a well-defined momentum. $|i\rangle$, $|f\rangle$, and $|j\rangle$ correspond to initial, final, and intermediate states, respectively. All intermediate states with photoexcited electrons in an upper band are virtual. The transition between $|j\rangle$ and $|j'\rangle$ states in (b) occurs due to the screened Coulomb interaction. Bold electron level lines show the Fermi energy.

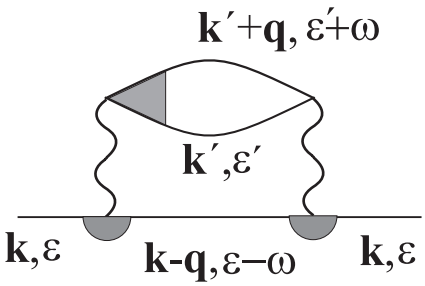

Figure 4. The Feynman graph for the contribution of the electron–electron interaction in the electron self-energy $\Sigma(\boldsymbol{k}, \varepsilon)$ in a metal with impurities, $\Sigma''(\boldsymbol{k}, \varepsilon) \propto 1/\tau_{ee}(\varepsilon)$. The grey triangle and half-circles show the renormalization by impurities. This contribution can be safely neglected in the calculation of the zero-momentum Raman response, since for any realistic system parameters $1/\tau_{ee}(\varepsilon \sim 1/\tau) \ll 1/\tau$ [6].

within the random-phase approximation:

$$V(Q, \omega_m) = \frac{V_0(Q)}{1 - V_0(Q) D(Q, \omega_m)}, \qquad V_0(Q) = \frac{4\pi e^2}{Q^2}, \tag{5}$$

with the square of the electron charge e^2 renormalized by the dielectric constant ϵ. The density–density correlation function $D(Q, \omega_m)$ has the form

$$D(Q, \omega_m) = N_F \left[\omega_m \tau \frac{\xi_v}{1 - \xi_v} - 1 \right], \tag{6}$$

with a parameter which corresponds to the impurity renormalization of the vertex in the ladder approximation:

$$\xi_v = \frac{\mathrm{i}}{2Q\ell} \ln \frac{z_1 + v_F Q}{z_1 - v_F Q}, \tag{7}$$

where $z_1 = \mathrm{i}(1/\tau + \omega_m)$. To obtain the susceptibility $\chi_Q(\omega_m)$, we integrate over the momenta of intermediate states and perform the summation over the intermediate Matsubara parameters

n_l and n_r in the outer loops corresponding to the virtual excitations coupled to the light via the non-fully symmetrical Raman vertex in figure 2, and n, which corresponds to the real excitation. After the integration, the result for the diffuson contribution has the form

$$\chi_{\mathcal{D}}(\omega_m) = T^2 \frac{\mathrm{i}}{v_F} \langle U^2(\boldsymbol{r})\rangle N_F \langle \gamma_{\boldsymbol{k}}^2 \rangle_{FS} \int \frac{\mathrm{d}Q}{(2\pi)^2}\, Q^2 \frac{V(Q,\omega_m)V^*(Q,\omega_m)}{(1-\xi_v)^2} D(Q,\omega_m) \times \int \mathrm{d}\theta \sin\theta \int \frac{\mathrm{d}K}{2\pi} K \sum_{n_l,n_r=-m}^{n_l,n_r=-1} \frac{\mathcal{D}(z_1,z_2;K,\boldsymbol{Q})}{1-\xi_{rn}}, \tag{8}$$

where $\boldsymbol{K} = |\boldsymbol{p}_l - \boldsymbol{p}_r|$, with $\boldsymbol{p}_l$ and $\boldsymbol{p}_r$ shown in figure 2, $\langle U^2\rangle = 1/\pi N_F \tau$ is the average square of the random potential, θ is the angle between $(\boldsymbol{p}_l + \boldsymbol{p}_r)/2$ and $\boldsymbol{Q}$, and the parameter for the rung of the ladder

$$\xi_{rn} = \frac{\mathrm{i}}{2K\ell} \ln \frac{z_1 + z_2 + \Omega_K}{z_1 + z_2 - \Omega_K}, \tag{9}$$

where $z_2 = \mathrm{i}(\varepsilon_r - \varepsilon_l)$. The ladder diagrams give the factor

$$\mathcal{D}(z_1,z_2;K,\boldsymbol{Q}) = \frac{2}{z_1[z_1^2 - \Omega_Q^2]} \left\{ \frac{1}{z_1 + 2\Omega_Q} \ln \frac{(z_2 - \Omega_Q + \Omega_K)(z_2 + z_1 + \Omega_Q - \Omega_K)}{(z_2 - \Omega_Q - \Omega_K)(z_2 + z_1 + \Omega_Q + \Omega_K)} + \frac{1}{2z_1} \ln \frac{(z_2 + z_1 + \Omega_K)(z_2 - z_1 - \Omega_K)}{(z_2 + z_1 - \Omega_K)(z_2 - z_1 + \Omega_K)} \right\}, \tag{10}$$

where $\Omega_Q = \boldsymbol{v}_F \boldsymbol{Q}$ and $\Omega_K = v_F K$.

Since the summation for the Cooperon contribution starts with two crossed impurity lines in the cross-section (see figure 2), the susceptibility contains one more ξ_{rn}-factor:

$$\chi_{\mathcal{C}}(\omega_m) = T^2 \frac{\mathrm{i}}{v_F} \langle U^2(\boldsymbol{r})\rangle N_F \langle \gamma_{\boldsymbol{k}}^2 \rangle_{FS} \int \frac{\mathrm{d}Q}{(2\pi)^2}\, Q^2 \frac{V(Q,\omega_m)V^*(Q,\omega_m)}{(1-\xi_v)^2} D(Q,\omega_m) \times \int \mathrm{d}\theta \sin\theta \int \frac{\mathrm{d}K}{2\pi} K \sum_{n_l,n_r=-m}^{n_l,n_r=-1} \mathcal{C}(z_1,z_2;K,\boldsymbol{Q}) \frac{\xi_{rn}}{1-\xi_{rn}}, \tag{11}$$

with

$$\mathcal{C}(z_1,z_2;K,\boldsymbol{Q}) = \frac{3z_1 - \Omega_Q}{4z_1^2(z_1 - \Omega_Q)^2(2z_1 - \Omega_Q)} \ln \frac{z_2 - z_1 + \Omega_Q + \Omega_K}{z_2 - z_1 + \Omega_Q - \Omega_K} - \frac{1}{\Omega_Q} \left[\frac{1}{z_1^2(z_1 - 2\Omega_Q)} \ln \frac{z_2 + \Omega_Q + \Omega_K}{z_2 + \Omega_Q - \Omega_K} - \frac{1}{z_1(z_1 - \Omega_Q)^2} \ln \frac{z_2 + \Omega_K}{z_2 - \Omega_K} \right] + \frac{1}{\Omega_Q^2} \left[\frac{1}{4z_1^2} \ln \frac{z_1 + z_2 + \Omega_Q + \Omega_K}{z_1 + z_2 + \Omega_Q - \Omega_K} - \frac{1}{z_1(2z_1 - \Omega_Q)} \ln \frac{z_1 + z_2 + \Omega_K}{z_1 + z_2 - \Omega_K} - \frac{3\Omega_Q - z_1}{4(z_1 - \Omega_Q)^2(z_1 - 2\Omega_Q)} \ln \frac{z_1 + z_2 - \Omega_Q + \Omega_K}{z_1 + z_2 - \Omega_Q - \Omega_K} \right], \tag{12}$$

where $\boldsymbol{K} = |\boldsymbol{p}_l + \boldsymbol{p}_r|$, and θ is the angle between $(\boldsymbol{p}_l - \boldsymbol{p}_r)/2$ and $\boldsymbol{Q}$.

Two dimensionless parameters determine the susceptibility $\chi_Q(\omega_m)$. The first one is $k_F\ell$, which depends on the disorder and shows how close the system is to the Anderson transition [12]. The second parameter, κ^2/k_F^2, describes the Coulomb interaction, where the Thomas–Fermi screening parameter $\kappa^2 = 4\pi e^2 N_F$. The results of numerical calculations for the diffuson and the Cooperon terms are presented in figure 5, where the analytical continuation $\mathrm{i}\omega_m \to \Omega + \mathrm{i}0$ was performed numerically with the Padé approximants [13]. As we can see in figure 5, the contribution of finite-momentum excitations to the spectral density of scattered light depends strongly on the Coulomb interaction between the electrons. The contribution of

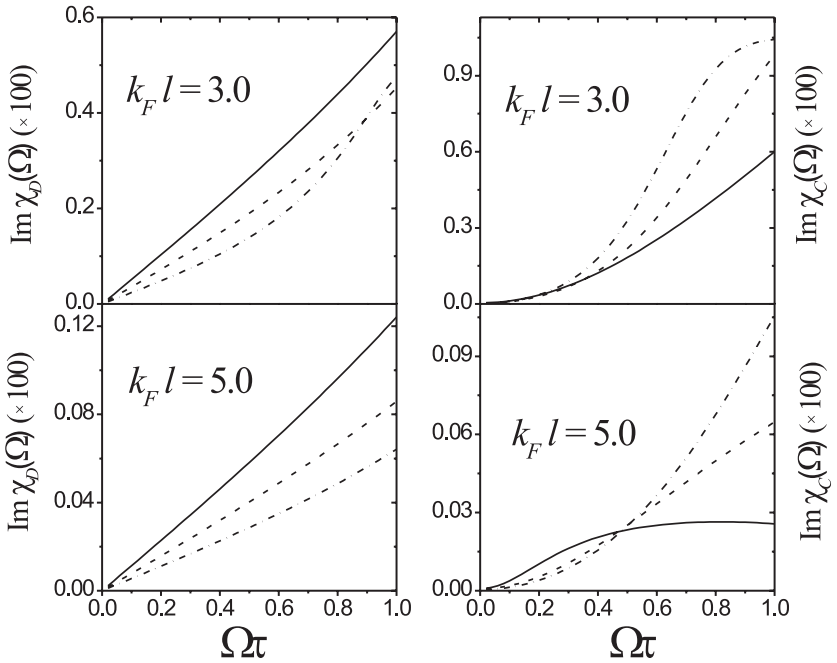

Figure 5. The contribution of the finite-momentum Raman process to the spectral density of the scattered light for different $k_F\ell$ and κ^2/k_F^2. Left panel: the diffuson contribution; right panel: the Cooperon contribution (in arbitrary units). Solid, dashed, and dash–dotted curves correspond to $\kappa^2/k_F^2 = 4$, $\kappa^2/k_F^2 = 2$, and $\kappa^2/k_F^2 = 1$, respectively. The temperature $T = 0.015\tau^{-1}$. The contribution of the zero-momentum process χ_0 in these units is $\Omega/(1+\Omega^2)$ (see equation (4)).

the finite-momentum excitations increases with decrease of $k_F\ell$ when the system approaches the metal–insulator transition of Anderson's type.

The effect considered in this paper is rather weak, leading to a correction less than 0.1 of the main zero-momentum contribution, since the localization effects are small in 3D metals and semiconductors. (The contribution of more complicated diagrams, as is known from the weak-localization theory, is small in comparison with this one, as it is proportional to $1/k_F\ell$.) However, it can be enhanced by the reduced dimensionality of the system, such as in two-dimensional quantum wells and one-dimensional quantum wires, where localization corrections to conductivity, $\Delta\sigma(\omega)$ diverge as $\ln(\omega\tau)$ and $1/\sqrt{\omega\tau}$, respectively. For these systems the role of correlations and disorder is larger than for 3D metals. The Raman scattering in these low-dimensional systems attracts a lot of experimental [14, 15] and theoretical attention [16, 17], mainly concentrated on the spectra of one-particle and collective excitations. The role of disorder in Raman scattering in low-dimensional systems still requires additional study. It is possible that properties of the Raman scattering in these systems that are not yet well understood can arise due to disorder [15], which causes localization, thereby enhancing the role of finite-momentum excitations. This problem remains to be investigated.

To conclude, we have considered Raman-active finite-momentum excitations in non-fully symmetrical scattering channels. These excitations arise due to the Coulomb interaction between the electrons. The contribution of these excitations is small in the range of frequencies described by the conventional model of the Raman scattering in metals with impurities [2]. Their role can be enhanced in low-dimensional systems such as two-dimensional electron gases

and quantum wires, where electron–electron interaction and disorder play a more important role than in 3D metals and semiconductors.

Acknowledgments

E Ya Sherman is grateful to V K Dugaev, Y Ito, and L A Maximov for valuable discussions and the Austrian Science Fund for support of the project P15520. O V Misochko acknowledges the support of RFBR grant 01-02-1640.

References

[1] Klein M V 1975 *Light Scattering in Solids* ed M Cardona (New York: Springer) p 147
[2] Zawadowski A and Cardona M 1990 *Phys. Rev.* B **42** 10732
[3] Falkovsky L A 1989 *Zh. Eksp. Teor. Fiz.* **95** 11 (Engl. transl. 1989 *Sov. Phys.–JETP* **68** 661)
[4] Shuker R and Gammon R W 1970 *Phys. Rev. Lett.* **25** 222
[5] Itai K 1992 *Phys. Rev.* B **45** 707
[6] Altshuler B L, Aronov A G, Khmelnitskii D E and Larkin A I 1982 *Quantum Theory of Solids* ed I M Lifshits (Moscow: Mir) p 130
[7] Abrikosov A A and Genkin V M 1973 *Zh. Eksp. Teor. Fiz.* **65** 842 (Engl. transl. 1974 *Sov. Phys.–JETP* **38** 417)
[8] Platzman P M 1965 *Phys. Rev.* A **139** 379
[9] A comprehensive analysis of the relation between the measured values and intrinsic properties of metals and semiconductors as well as the description of the formalism can be found, for example, in the review papers
Einzel D and Hackl R 1996 *J. Raman Spectrosc.* **27** 307
Devereaux T P and Kampf A P 1997 *Int. J. Mod. Phys.* **11** 2093
and in [1].
Sherman E Ya, Misochko O V and Lemmens P 2003 *Spectroscopy of High T_c Superconductors* ed N M Plakida (London: Taylor and Francis) p 97
[10] The importance of this kind of Raman process for light scattering in strongly correlated layered high-T_c superconductors was suggested by
Klein M V, Cooper S L, Kotz A L, Liu R, Reznik D, Slakey F, Lee W C and Ginsberg G M 1991 *Physica* C **185–189** 72
[11] The shake-up of the atomic shells as the mechanism of inelastic scattering of x-rays in insulating cuprates was considered in
Abbamonte P, Burns C A, Isaacs E D, Platzman P M, Miller L L, Cheong S W and Klein M V 1999 *Phys. Rev. Lett.* **83** 860
[12] Recently, the Raman scattering via the metal–insulator transition induced by electronic correlations was considered within the Falicov–Kimball model in
Freericks J K and Devereaux T P 2001 *Phys. Rev.* B **64** 125110
Freericks J K, Devereaux T P and Bulla R 2001 *Phys. Rev.* B **64** 233114
[13] Vidberg H J and Serene J W 1977 *J. Low Temp. Phys.* **29** 179
[14] Steinebach C, Krahne R, Biese G, Schüller C, Heitmann D and Eberl K 1996 *Phys. Rev.* B **54** R14281
[15] Jusserand B, Vijayaraghavan M N, Laruelle F, Cavanna A and Etienne B 2000 *Phys. Rev. Lett.* **85** 5400
[16] Mariani E, Sassetti M and Kramer B 2000 *Europhys. Lett.* **49** 224
[17] Das Sarma S and Wang D W 1999 *Phys. Rev. Lett.* **83** 816
Wang D W and Das Sarma S 2002 *Phys. Rev.* B **65** 035103